CORROSION SCIENCE AND TECHNOLOGY, Vol.7, No.6(2008), pp.301~306

Hardness and Corrosion Resistance of Surface Composites Fabricated with Fe-based Metamorphic Powders by High-energy Electron Beam Irradiation

Dukhyun Nam, Kyuhong Lee, Sunghak Lee†, and Kyoo Young Kim

Center for Advanced Aerospace Materials
Pohang University of Science and Technology, Pohang, 790-784 Korea

Surface composite layers of 1.9~2.9 mm in thickness were fabricated by depositing metamorphic powders on a carbon steel substrate and by irradiating with a high-energy electron beam. In the surface composite layers, 48~64 vol.% of Cr_2B or $Cr_{1.65}Fe_{0.35}B_{0.96}$ borides were densely precipitated in the austenite or martensite matrix. These hard borides improved the hardness of the surface composite layer. According to the potentiodynamic polarization test results of the surface composites, coatings, STS304 stainless steel, and carbon steel substrate, the corrosion potential of the surface composite fabricated with 'C+' powders was highest, and its corrosion current density was lowest, while its pitting potential was similar to that of the STS304 steel. This indicated that the overall corrosion resistance of the surface composite fabricated with 'C+' powders was the best among the tested materials. Austenite and martensite phases of the surface composites and coatings was selectively corroded, while borides were retained inside pits. In the coating fabricated with 'C+' powders, the localized corrosion additionally occurred along splat boundaries, and thus the corrosion resistance of the coating was worse than that of the surface composite.

Keywords *: high-energy electron beam irradiation, surface composite, metamorphic powder, corrosion resistance.*

1. Introduction

From the reports1)to4), as steels have been increasingly exposed to severe industrial working environments, steel-based surface composites, in which advantages of amorphous alloys or ceramics having excellent resistance to wear and corrosion are fully taken by direct irradiation of high-energy electron beam, have received attentions. Upon irradiating a steel surface with a high-energy electron beam, high kinetic energy of electrons is transformed to high thermal energy, which can easily melt amorphous alloys or ceramics. When a steel substrate, on which amorphous alloy or ceramic powders are evenly deposited, is irradiated with an electron beam, both powders and the surface region of the substrate are melted. In this process, amorphous or ceramic phases are dispersed and infiltrated into the substrate, thereby fabricating steel-based surface composites. From the reports5),6), this high-energy electron-beam irradiation has advantages of a strong interface between the surface composite layer and substrate and of a continuous process in the air. Thus, if the fabrication method of steel-based surface composites, in which the surface region consists of amorphous alloys or ceramics and the interior substrate consists of a ductile steel having sufficient ductility and fracture toughness, can be developed, advantages of amorphous alloys or ceramics are taken in the fabricated steel-based surface composites. Commercial Fe-based metamorphic powders containing a considerable amount of crystalline phases are strong candidates as reinforcing powders of the steel-based surface composites. From the reports7)to9), they consist of both amorphous and crystalline phases, and are generally used as thermal spray coating powders to improve wear and corrosion resistance. In the present study, steel-based surface composites were fabricated by evenly depositing Fe-based metamorphic powders on a plain carbon steel substrate and irradiating a high-energy electron beam to improve surface properties of a steel substrate. The microstructure, hardness, and corrosion resistance of the fabricated surface composites were investigated, and compared with those of a coating sprayed with same metamorphic powders.

† Corresponding author: shlee@postech.ac.kr

2. Experimental

Two kinds of Fe-based metamorphic powders, i.e., Armacor™ 'C+' and 'M' which are commercial brand names of the Liquidmetal Technologies, Lake Forest, CA, U.S.A., were used for the fabrication of steel-based surface composites. Their chemical compositions were Fe-30Cr-17Ni-10Co-4Mo-4B-2.5Cu-1.5Si (wt.%) and Fe-43Cr-5.6B-1.8Si-0.2S-0.17C(wt.%), respectively, and the average powder size was about 50 μm. These powders were dried at 150℃ for 2 hrs, evenly deposited on a plain carbon steel substrate (thickness; 15 mm), and then pressed with a 120 kPa load using a mold. A high-energy electron accelerator at the Budker Institute of Nuclear Physics, Novosibirsk, Russia, was used for the irradiation under optimally fixed process conditions (electron energy; 1.4 MeV, specimen moving speed; 35 mm/sec, scanning width; 50 mm, beam current; 55 mA, beam diameter; 11 mm) without using a flux. Powders were deposited once again on the one-layered surface composites fabricated by the one-time electron beam irradiation, and then irradiated by high-energy electron beam to fabricate two-layered surface composites. In addition, thermal sprayed coatings were fabricated with 'C+' and 'M' powders by a high-velocity oxygen fuel (HVOF) spray method. For convenience, the surface composite specimens or coatings fabricated with 'C+' and 'M' powders are referred to as 'C' and 'M' specimens or 'C' and 'M' coatings, respectively.

Hardness was measured by a Vickers hardness tester under a 300 g load. Open circuit potential (OCP) measurements and potentiodynamic polarization tests were conducted in an aerated 3.5% NaCl solution at room temperature. A saturated calomel electrode (SCE) was used as a reference electrode, and two parallel high-density graphite rods were served as counter electrodes for the current measurement. The OCP was measured after a delay of 30 minutes for the specimens to reach a steady state. Then, the specimen was potentiodynamically polarized at a scan rate of 1 mV/s from 0.25 V below the OCP to 1.2 V above the SCE potential.

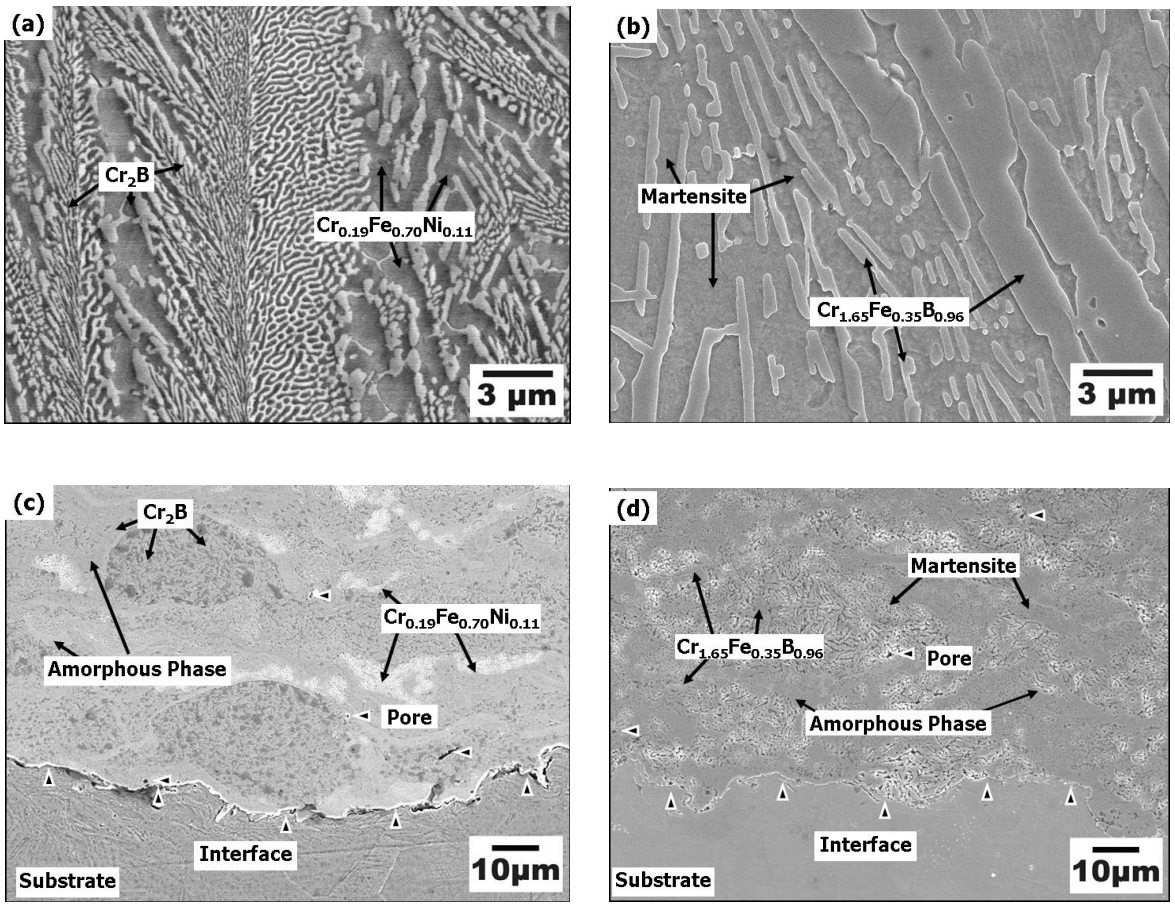

Fig. 1. SEM micrographs of the (a) C and (b) M specimens and the (c) C and (d) M coatings, showing surface composite layers or coated layers. Etched by Viella solution.

Table 1. Quantitative analysis results of the surface composites and sprayed coatings.

Specimen	Layer Thickness [mm]	Volume Fraction [%]				
		Boride	Austenite	Martensite	Amorphous Phase	Pore
C Specimen	1.87	47.7	52.3	-	-	-
M Specimen	2.91	63.9	-	36.1	-	-
C Coating	0.22	67.8	24.2	-	5.0	2.0
M Coating	0.21	75.5	-	20.4	2.8	1.3

3. Reseult and discussion

3.1 Microstructure

The C and M specimens show smooth surface composite layers without defects such as pores or cracks. The surface composite layer/substrate interface is clearly visible. The interface between the first and second composite layers is not observed because the residual first layer was completely melted by the two-time electron beam irradiation. The thicknesses of the surface composite layers of the C and M specimens are 1.9 mm and 2.9 mm, respectively. SEM micrographs of the C and M specimens and C and M coatings are shown in Figs. 1(a) through (d). The surface composite layers of the C and M specimens are generally composed of densely precipitated crystalline particles and matrix phase (Figs. 1(a) and (b)). Volume fraction of crystalline precipitates in the M specimen is 64 %, which is higher than that of the C specimen (48%). In the C and M coatings of 0.2 mm in thickness, elongated splats form a curved lamellar structure (Figs. 1(c) and (d)).

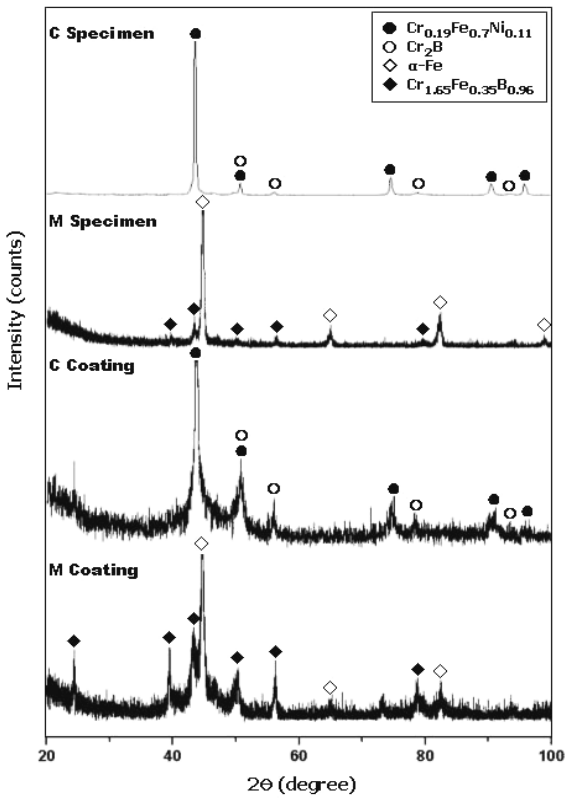

Fig. 2. X-ray diffraction patterns of the C and M specimens and the C and M coatings.

Phases in the surface composite layers and coatings were analyzed by the XRD (Fig. 2). Sharp diffraction peaks of crystalline phases are observed in the C and M specimens. This indicates the presence of crystalline phases without amorphous phases. Peaks of austenite and Cr_2B are observed in the C specimen, while peaks of $Cr_{1.65}Fe_{0.35}B_{0.96}$ and *α*-Fe are found in the M specimen. Peaks of *α*-Fe might be ones of martensite formed by fast cooling. Thus, $Cr_{1.65}Fe_{0.35}B_{0.96}$ or Cr_2B borides are distributed in the austenite or martensite matrix for the C and M specimens, respectively, as shown in Figs. 1(a) and (b). In the C and M coatings, sharp diffraction peaks of crystalline phases as well as broad halo patterns are observed. According to the EDS analysis data of the C coating, light-gray, dark-gray, and white regions, as indicated by arrows in Fig. 1(c), are identified to be Cr_2B, austenite, and amorphous phases, respectively. In the M coating, $Cr_{1.65}Fe_{0.35}B_{0.96}$, martensite, and amorphous phases are found as indicated by arrows in Fig. 1(d). Volume fractions of observed phases are listed in Table 1.

3.2 Hardness

The hardness of the surface composite layers and coatings are shown in Table 2. The hardness of the surface composite layer of the C specimen is about 480 VHN, which is 2.5 times higher than that of the carbon steel substrate (200 VHN). The hardness of the surface composite layer of the M specimen is higher than that of the C specimen because of the higher volume fraction of hard borides. The hardness of the coatings is higher than that of the surface composite layers. The hardness of the M coating is higher than that of the C coating.

3.3 Corrosion resistance

Fig. 3 shows potentiodynamic polarization curves of the surface composite layers and coatings, together with a con

Table 2. Vickers hardness and potentiodynamic polarization test results of the surface composites and sprayed coatings.

Specimen	Hardness [VHN]	Corrosion Potential(E_0) [V_{SCE}]	Corrosion Current Density (i_0) [$\mu A/cm^2$]	Pitting Potential (E_{pit}) [V_{SCE}]
C Specimen	483±15	-0.130	0.037	0.146
M Specimen	583±26	-0.198	0.305	-0.028
C Coating	721±82	-0.196	0.170	0.029
M Coating	899±94	-0.194	0.150	-
Steel Substrate	197±8	-0.472	5.360	-
STS304 Stainless Steel	-	-0.252	0.136	0.150

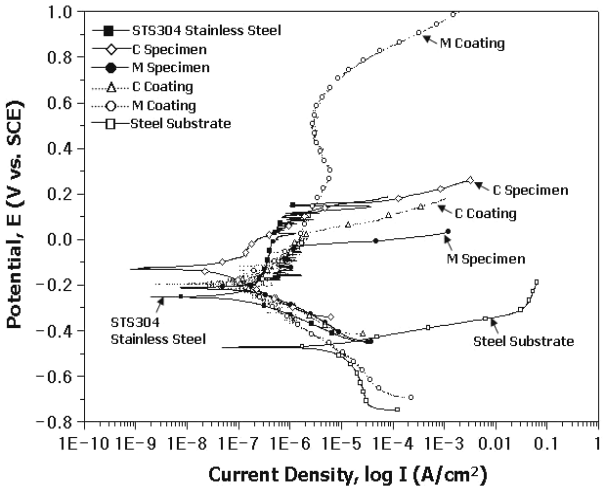

Fig. 3. Potentiodynamic polarization curves of the C and M specimens, C and M coatings, STS304 stainless steel, and steel substrate.

ventional STS304 stainless steel and a steel substrate. Corrosion potential (E_o), corrosion current density (i_o), and pitting potential (E_{pit}) obtained from the polarization curves are shown in Table 2. i_o is lowest in the C specimen, and increases in the order of the STS304 steel, M coating, C coating, and M specimen, which indicates that the C specimen can show the best corrosion resistance. E_o is highest in the C specimen, and decreases in the order of the M coating, C coating, M specimen, and STS304 steel. It can be concluded from Table 2 that the overall corrosion resistance of the C specimen is the best. In view of the pitting corrosion, the C specimen is similar to the STS304 steel, and is better than the M specimen and C coating.

Figs. 4(a) through (f) show corroded surfaces. Pits are formed on the corroded surfaces of the C and M specimens and C coating (Figs. 4(a) through (c)). In the C specimen composed of Cr_2B and austenite, the one phase was retained inside pits, while the other phase was selectively corroded (Fig. 4(d)). According to the EDS analysis, the phase retained inside pits is found to be Cr_2B. Cr_2B and austenite phases act as a cathode and an anode, respectively, and the austenite matrix is selectively corroded. Pits of the M specimen are deeper than those of the C specimen (Fig. 4(b)). Inside deep pits, only $Cr_{1.65}Fe_{0.35}B_{0.96}$ borides are observed without martensite (Fig. 4(e)), indicating that the martensite matrix works as an anode and selectively corrodes. The galvanic corrosion potential of the austenite matrix in the C specimen might be higher than that of the martensite matrix in the M specimen since the austenite phase has good corrosion resistance, while the martensite is a steel phase which can be easily corroded. Thus, the resistance to overall corrosion including pitting corrosion of the M specimen is lower than that of the C specimen, and pits are deeper in the M specimen. Only Cr_2B borides are observed inside pits without austenite or amorphous phases in the C coating (Fig. 4(f)). Austenite and amorphous phases are corroded, while Cr_2B borides are retained. Considering that the fraction of Cr_2B is higher in the C coating than in the C specimen, the corrosion resistance of the C coating might be better, but the corrosion test results show the opposite trend. In the C coating, elongated splats form a curved lamellar structure, and about 2 vol.% of pores or cracks exist mainly along splat boundaries (Fig. 1(c)). Thus, it is possible that the localized corrosion can occur along pores or cracks located mainly along splat boundaries. Since the localized corrosion along splat boundaries as well as the selective corrosion occur inside pits of the C coating, a considerable number of splats are spalled out or corroded. The C coating shows the mixed corrosion mode of the localized corrosion and galvanic corrosion, and its overall corrosion resistance is worse than that of the C specimen.

4. Summary

In the steel-based surface composites, Cr_2B of $Cr_{1.65}Fe_{0.35}B_{0.96}$ borides having good hardness and corrosion resistance are homogeneously distributed in the austenite or martensite matrix, thereby resulting in the improvement of the overall hardness and corrosion resistance. Particularly, the C specimen has the better corrosion resistance than the C coating containing more Cr_2B borides because the localized corrosion does not occur in the C specimen.

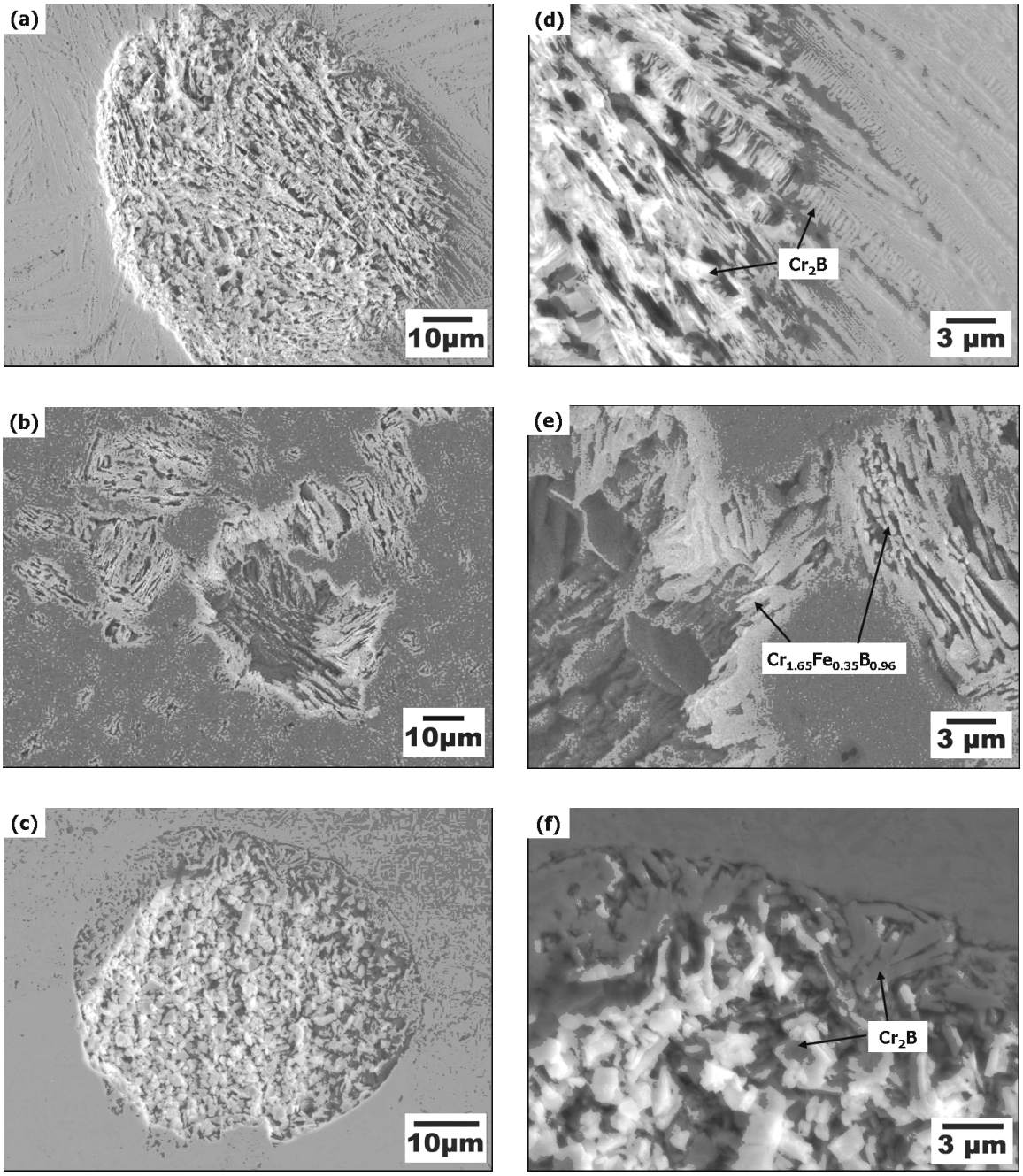

Fig. 4. SEM micrographs of pits formed on the corroded surface of the (a) C and (b) M specimens and the (c) C coating after the potentiodynamic polarization test. (d) through (f) are high-magnification SEM micrographs of pits of (a) through (c), respectively.

Since the austenite matrix in the C specimen is selectively corroded by forming a galvanic coupling, the pitting corrosion resistance of the C specimen is deteriorated, but keeps an excellent level similar to that of the STS304 stainless steel having a single austenite phase. Considering the overall corrosion properties, the C specimen has the best corrosion resistance among the surface composites, coatings, and STS304 steel. Furthermore, the C specimen has advantages of a strong interfacial bonding between surface composite layer and substrate and of elimination of defects such as pores or cracks, whereas coatings generally have defects and interfacial bonding problems. Thus, the C specimen shows excellent hardness and corrosion resistance due to the hardening and corrosion-resistant effects

of Cr_2B borides, and presents good application possibilities as excellent wear- and corrosion-resistant materials.

Acknowledgments

This work was supported by the National Research Laboratory Program funded by the Korea Science and Engineering Foundation (KOSEF). Authors are grateful to the Liquidmetal Technologies for supplying Fe-based metamorphic powders and Drs. M.G. Golkovski and N. Kuksanov of Budker Institute of Nuclear Physics for their helpful discussion on the fabrication of the surface composites.

References

1. J. E. Krzanowski and R. E. Leuchtner, *J. Am. Ceram. Soc*., **80**, 1277 (1997).
2. Y. Herrera, I. C. Grigorescu, J. Ramirez, C. Di Rauso, and M.H. Staia, *Surf. Coat. Technol*., **108-109**, 308 (1998).
3. D. I. Pantelis, E. Bouyiouri, N. Kouloumbi, P. Vassiliou and A. Koutsomichalis, *Surf. Coat. Technol*., **298**, 125 (2002).
4. K. Euh and S. Lee, *Metall. Mater. Trans. A*, **34**, 59 (2003).
5. K. Euh, Y. C. Kim, K. Shin, S. Lee, and N. J. Kim, *Mater. Sci. Eng. A*, **346**, 228 (2003).
6. K. Lee, D.-H. Nam, and S. Lee, *J. Kor. Inst. Met. & Mater*., **43**, 172 (2005).
7. H. Y. Wang, L Huang, and Q.C. Jiang, *Mater. Sci. Eng. A*, **407**, 98 (2005).
8. R. C. Tucker, Advances in coating Technologies for corrosion and wear resistance coating, p. 89, TMS (2005).
9. P. De la Cruz and T. Ericsson, *Mater. Sci. Eng. A*, **247**, 204 (1998).